Identification of the P-Loop Lysine as a Metal Ligand in the Absence of Nucleotide at Catalytic Site 3 of Chloroplast F_1-ATPase from *Chlamydomonas reinhardtii*†

Donald J. Crampton, Russell LoBrutto, and Wayne D. Frasch*

The Center for the Study of Early Events in Photosynthesis, Arizona State University, Tempe, Arizona 85287-1601

Received December 20, 2000; Revised Manuscript Received January 31, 2001

ABSTRACT: Site-directed mutations were made to the phosphate-binding loop lysine in the β-subunit of the chloroplast F_1-ATPase in *Chlamydomonas reinhardtii* (βK167) to investigate the participation of this residue in the binding of metal to catalytic site 3 in the absence of nucleotide. The cw-EPR spectra of VO^{2+} bound to site 3 of CF_1-ATPase from wild type and mutants revealed changes in metal ligation resulting from mutations to βK167. The three-pulse ESEEM spectrum of the wild-type CF_1-ATPase with VO^{2+} bound to site 3 shows an equatorially coordinating ^{14}N from an amine. The ESEEM spectra of the mutants do not show evidence of an equatorially coordinating amine group. The results presented here show that, in the absence of nucleotide, βK167 is a ligand to the metal bound at catalytic site 3, suggesting a regulatory role for the P-loop lysine in addition to its known role in catalysis.

The F_1F_0-ATP synthase uses a nonequilibrium transmembrane proton gradient to synthesize ATP from ADP and phosphate, thereby forming a nonequilibrium chemical gradient of products versus substrates (*1*). The F_1[1] portion binds substrate with high affinity in a manner that allows rapid interconversion of ADP and phosphate with bound ATP in the absence of the protonmotive force (*2*). The protonmotive force drives two sequential conformational changes of the catalytic site that decrease the affinity of the enzyme for ATP relative to ADP, thereby facilitating the selective dissociation of ATP to generate the chemical gradient. The conformation of each of three catalytic sites on the enzyme is staggered such that the enzyme contains a catalytic site in each of the three conformations at any instant.

Nucleotides bind to catalytic sites as a complex with Mg^{2+} that serves as a cofactor for hydrolysis (*3*). The conformations of each of the three catalytic sites in the crystal structure of F_1-ATPase from bovine heart mitochondria differ (*4*). One site contains Mg^{2+}-AMPPNP (β_{TP}), one has bound Mg^{2+}-ADP (β_{DP}), and one is empty (β_E). However, when crystallized with nucleotide in the absence of Mg^{2+}, the $\alpha_3\beta_3$ portion of the rat liver mitochondrial F_1-ATPase shows 3-fold symmetry despite the presence of the γ-subunit (*5*).

The Mg^{2+} not only induces structural asymmetry of the catalytic sites, but also is responsible for large differences in nucleotide affinities (*6*). In the absence of Mg^{2+}, the three catalytic sites of *Esherichia coli* F_1-ATPase bind ATP with the same affinity. In contrast, when ATP binds as a complex with Mg^{2+}, the affinity for nucleotides at the three catalytic sites can differ by as much as 5 orders of magnitude. This suggests that the differences in affinity may result in part from changes in the metal ligands during the conformational changes at the catalytic sites.

The catalytic activity of chloroplast F_1 (CF_1) separated from F_0 and the thylakoid membrane is latent, although ATPase activity can be activated via reduction of a disulfide bond on the γ-subunit (*7*). The oxidation state of this disulfide provides one of multiple levels of interrelated mechanisms to regulate the enzyme to minimize ATPase activity once the proton gradient dissipates in the absence of light-driven proton translocation. The dark decay of ATPase activity in thylakoids is accelerated by the addition of ADP that becomes tightly bound in the latent state (*8*−*10*). Formation of this tightly bound ADP and inhibition of ATPase activity only occur upon the addition of Mg^{2+} (*11*). Under these conditions, Mg^{2+} induces the formation of an entrapped Mg^{2+}-ADP complex at a high-affinity catalytic site. This binding of Mg^{2+}-ADP has been found to serve a regulatory function in the F_1-ATPases from other organisms as well (*12*, *13*). The tightly bound Mg^{2+}-ADP must be released from the catalytic site before the enzyme can be fully active (*14*−*16*).

The binding of Mg^{2+} in the absence of nucleotide strongly inhibits the ATPase activity of purified F_1-ATPases (*17*, *18*) by a process known as free-metal inhibition. The ATPase activity of F_1-ATPase from *E. coli* and lettuce chloroplasts shows activation as divalent metal concentration initially increases with respect to ATP and then inhibition at higher metal:ATP concentration ratios (*19*, *20*). The binding of inhibitory Mg^{2+} has been shown to be competitively inhibited by H^+ within the pH interval 6.8−8.2 (*21*, *22*). Inhibition by entrapped Mg^{2+}-ADP has been found to increase as a result of the binding of free Mg^{2+} at other sites when the

† This work was supported by National Institutes of Health Grant GM50202 to W.D.F. and National Science Foundation Equipment Grant BIR-9601774 to R.L.

* To whom correspondence should be addressed. E-mail: frasch@asu.edu. TEL: (480) 965-8663. FAX: (480) 965-6899.

[1] Abbreviations: F_1, the extrinsic membrane portion of the F_1F_0-ATP synthase; CF_1, chloroplast F_1; EF_1, *E. coli* F_1; MF_1, mitochondrial F_1; P-loop, phosphate-binding loop; cw-EPR, continuous wave electron paramagnetic resonance; ESEEM, electron spin echo envelope modulation.

10.1021/bi002895y CCC: $20.00
Published on Web 02/24/2001

inhibitory Mg^{2+}-ADP is already bound (*23*). Consequently, it has been postulated that free-metal inhibition results from an increased amount of entrapped Mg^{2+}-ADP (*24*).

The catalytic sites of CF_1-ATPase are designated sites 4, 1, and 3 in order of decreasing affinity for Mg^{2+}-nucleotide (*25*, *26*). Vanadyl has been used as a direct probe to identify the groups that serve as metal ligands at sites 1 and 3 of the latent and activated forms of the chloroplast F_1-ATPase (*27*−*29*). Vanadyl $(V^{IV}{=}O)^{2+}$ is a cation composed of vanadium-(IV) double-bonded to oxygen which results in a net charge of 2+. In its square-planar conformation, vanadyl has four equatorial ligands, and one axial ligand that is trans to the vanadium−oxygen bond. Vanadyl has a single unpaired electron ($S = 1/2$) and a nuclear spin $I = 7/2$. The combination of relatively weak *g*-anisotropy and an axially symmetric ^{51}V hyperfine coupling tensor gives rise to a 16-line cw-EPR spectrum. The principal values of the hyperfine coupling are sensitive to the type of groups that serve as equatorial ligands. Also, ESEEM spectroscopy of VO^{2+} sometimes allows the resolution of super-hyperfine coupling from ligated nuclei.

The titration of VO^{2+}-nucleotide to CF_1-ATPase that had been depleted of metal-nucleotide only from site 3 showed that the VO^{2+} had bound selectively to a single site (*30*). At site 3 in latent CF_1-ATPase from *Chlamydomonas reinhardtii*, the majority of VO^{2+}-nucleotide binds in a ligand environment that gives rise to cw-EPR species B ($A_{||} = 497.5$ MHz, $g_{||} = 1.9475$), whereas a smaller fraction binds to site 3 in a form that gives rise to EPR species C ($A_{||} = 456.5$ MHz, $g_{||} = 1.9575$) (*27*, *28*). In the absence of nucleotide, VO^{2+} bound to site 3 of CF_1-ATPase from spinach gives rise to a single cw-EPR species (*31*). The three-pulse ESEEM spectrum of the VO^{2+} bound to CF_1-ATPase in this manner contains two intense nuclear transition frequencies (*31*) that are typical of an ^{14}N nucleus from an equatorially coordinating amine group (*32*).

The P-loop lysine of F_1-ATPases is part of a highly conserved motif, GXXXXGKT/S, that has similar functions in many enzymes that bind nucleotides (*33*). When the Mg^{2+}-nucleotide complex is bound, the P-loop threonine coordinates the metal while the protonated amine of the P-loop lysine hydrogen bonds to the phosphate oxygens of the nucleotide that do not coordinate metal in the catalytic sites (*4*). Recently, the P-loop lysine has been demonstrated to be important for generation and stabilization of the catalytic transition state (*34*). If the amine group observed by ESEEM to be coordinated to the metal is the P-loop lysine, such an arrangement could interfere with the functional binding of nucleotide and contribute to inhibition of ATPase activity.

We have now characterized site-directed mutations of the P-loop lysine in the β-subunit of CF_1-ATPase from *Chlamydomonas reinhardtii* (βK167). The effects of these mutations on the cw-EPR and ESEEM spectra of VO^{2+} bound to site 3 of CF_1-ATPase were examined. All mutations changed the ^{51}V-hyperfine coupling of the free-metal-bound species significantly, and caused a substantial decrease in the intensities of the nuclear transition frequencies associated with an equatorially coordinating ^{14}N nucleus from an amine. The results indicate that βK167 contributes an amine group as an equatorial metal ligand when VO^{2+} binds to catalytic site 3 of CF_1-ATPase without nucleotide.

EXPERIMENTAL PROCEDURES

Construction of CF_1 Mutants in C. reinhardtii. The recombinant plasmid carrying the wild-type gene *atpB* of *C. reinhardtii* was constructed as described by Hu et al. (*35*). The 5.3-kb *Eco*RI−*Bam*HI fragment of the chloroplast genome containing *atpB* was cloned into pUC18, and then a 1.4-kb *atpA*−*aadA* cassette was inserted into the plasmid at a *Kpn*I site of the 5.3-kb fragment. The resulting recombinant plasmid known as pBam 10.3-spec was used as a template to make mutants. The *atpA*−*aadA* cassette included the promoter of the *atpA* gene and *aadA* that encodes a protein against the antibiotic spectinomycin.

Stratagene kit 200508 was used to generate *atpB* mutations on pBam 10.3-spec following the provided protocol that required two primers for each mutant. The mutagenesis primers were as follows:

βK167C, 5′-CGGTGGTGCCGGTGTAGGCTGTACA-GTTTTAATTATGG-3′

βK167G, 5′-CGGTGGTGCCGGTGTAGGCGGCACA-GTTTTAATTATGG-3′

βK167H, 5′-CGGTGGTGCCGGTGTAGGCCATACA-GTTTTAATTATGG-3′

βK167L, 5′-CGGTGGTGCCGGTGTAGGCTTAACA-GTTTTAATTATGG-3′

The mutagenesis primers each contained a silent mutation that introduced the *Msp*I restriction site. The selective primer that changed restriction site *Xmn*I to *Bam*HI was Ps (5′-CGCCCCGAAGAACGGATCCCAATGATGAGCAC-3′).

Sequences of DNA were obtained using ABI PRISM automatic sequencing to confirm the mutations in the plasmids. The sequence primer was 5′-CCGTACAGCTC-CTGCTTTCG-3′. The mutated plasmids were purified by ultracentrifugation with cesium chloride and diluted to 1 mg/mL.

The CC-373 and CC-125 strains of *C. reinhardtii* were obtained from the *Chlamydomonas* culture collection center at Duke University. The CC-373 strain has a 2.5-kb deletion that starts close to the 5′-end of *atpB*. The transformation of CC-373 with mutated pBam 10.3-spec was performed using the PDS-1000 particle delivery system (Dupont New England Nuclear) as described by Chen et al. (*28*). Southern blots were done as described by Chen et al. (*28*) using ^{32}P-labeled pBam 10.3-spec as the probe to determine that the mutants were homoplasmic. The presence of the desired mutation was confirmed by sequencing the PCR product from the chloroplast genome of each mutant.

Growth of C. reinhardtii Wild Type and Mutants. Cell cultures were maintained for each *C. reinhardtii* strain as per Hu et al. (*35*). The growth curves were determined by the change in optical density (cell scattering) at 720 nm under photoautotrophic growth conditions as per Hu et al. (*27*).

EPR Sample Preparation and EPR Measurements. To purify CF_1-ATPase from *Chlamydomonas* thylakoids, isolated thylakoids were incubated with 0.75 mM EDTA (pH 8.0) for 15 min at room temperature. The suspension was centrifuged at 30000*g* for 20 min to remove the thylakoids. This EDTA extraction was repeated 3 times. DEAE-Sephadex A-50 that had been preequilibrated in 20 mM

Tris−NaOH (pH 8.0), 10 mM ammonium sulfate, and 1 mM EDTA was added to the combined supernatants containing CF_1-ATPase. The suspension was stirred slowly for 30 min at room temperature and then loaded into a chromatography column. The protein was eluted from this column with 300 mL of buffer that contained 20 mM Tris−NaOH (pH 8.0), 1.0 mM ATP, 2 mM EDTA, and 500 mM NaCl. The fractions that contained CF_1-ATPase were concentrated by pressure dialysis using an Amicon YM-100 membrane to a volume of about 3 mL. It has been shown previously (*30*) that CF_1-ATPase purified in this manner contains about four tightly bound Mg^{2+}-nucleotides. The purified CF_1-ATPase was depleted of the Mg^{2+}-nucleotide from site 3 by chromatography on a 3 × 30 cm Sephadex G-50 column equilibrated in 50 mM HEPES (pH 8.0), 1 mM ATP, and 500 mM NaCl. The eluent was concentrated again via pressure dialysis using a YM-100 membrane to a volume of about 1 mL. The sample was then diluted in buffer containing 50 mM HEPES (pH 8.0) to a final NaCl concentration of 175 mM. This treatment has been shown to deplete CF_1-ATPase of site 3 bound nucleotide without removing significant amounts of metal-nucleotide from the other tight binding sites (*36*). The protein was concentrated to 0.3 mL, and the extinction coefficient of $\epsilon = 0.483$ cm^2 (mg of CF_1)$^{-1}$ (*25*) was used to determine the concentration. One mole equivalent of VO^{2+} was added to the site 3 nucleotide-depleted CF_1-ATPase samples as described by Houseman et al. (*31*).

A Bruker E580 spectrometer with a standard TE_{102} rectangular cavity and a liquid nitrogen flow cryostat operating at 125 K was used for cw-EPR experiments at X-band (9 GHz). Of the eight transitions that result from that fraction of enzyme-bound VO^{2+} where the axis (defined by the oxo bond) is aligned parallel with the magnetic field, the $-7/2_{||}$, $-5/2_{||}$, $+3/2_{||}$, $+5/2_{||}$, and $+7/2_{||}$ transitions do not overlap with the perpendicular transitions. The measurable parallel transitions are distributed over a magnetic field range well in excess of 1000 G, and the high nuclear spin multiplicity of ^{51}V amplifies any discrepancy between simulated and observed field positions for these transitions. Therefore, a set of hypothetical $A_{||}$ and $g_{||}$ values, derived from a simulation that fits all five parallel transitions well, can reasonably be expected to be both unique and quite accurate. Simulations for the present study were obtained using the program QPOWA [Houseman et al. (*31*)]; spectral parameters obtained from the simulations are given in Table 2.

To estimate the types of groups that serve as equatorial ligands to VO^{2+}, the observed value of $A_{||}$ derived from simulation was compared with values of $A_{||}$ calculated from the coupling constants obtained from model studies (*37*, *38*), by

$$A_{||calc} = \Sigma n_i A_{||i}/4 \quad (1)$$

where i counts the different types of equatorial ligand donor groups, n_i ($n_i = 1-4$) is the number of ligands of type i, and $A_{||i}$ is the measured coupling constant for the equatorial ligand donor group of type i. A similar equation can be written for $g_{||}$.

Three-pulse ESEEM was used to detect ^{14}N superhyperfine couplings to VO^{2+}. These experiments were carried out at 20 K using a Bruker 580E spectrometer, incorporating a variable-Q dielectric resonator operating at 9.7 GHz, and an Oxford ESR900 liquid helium flow cryostat. The time domain data record was zero-filled and Fourier-transformed. ESEEM spectra are presented in the frequency domain in absolute value form.

Table 1: Photoautotrophic Growth of Wild-Type and βK167 Mutants of *C. reinhardtii*

genotype	photoautotrophic growth rate[a] (%)
wild type	100
βK167C	14
βK167G	14
βK167H	25
βK167L	14

[a] Measured as the rate of increase in optical density (cell scattering) of the liquid culture at 720 nm in log phase at 25 °C with a light intensity of 80 μE M^{-2} s^{-1}.

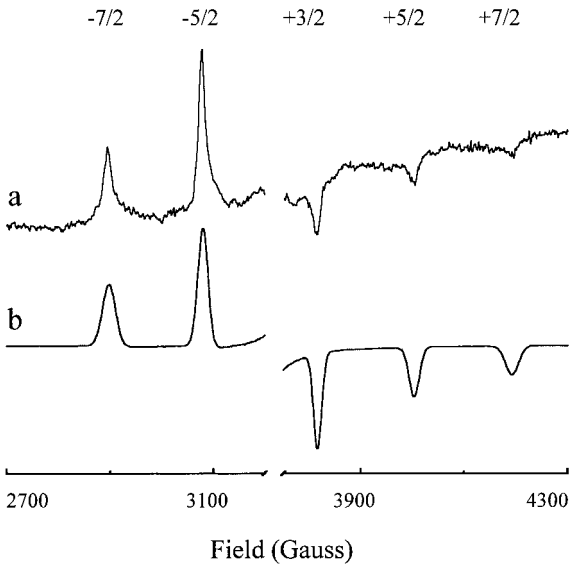

FIGURE 1: (a) Parallel regions of the cw-EPR spectrum of VO^{2+} bound in the absence of nucleotide to site 3 of latent CF_1-ATPase from wild-type *Chlamydomonas reinhardtii*. One mole equivalent of VO^{2+} was added to 54 mg of CF_1 as described under Experimental Procedures. EPR conditions were as follows: field modulation frequency, 100 kHz; modulation amplitude, 0.5 mT; sweep rate, 0.95 mT/s; time constant, 82 ms; microwave power, 2.0 mW; temperature, 125 K; microwave frequency, 9.660 GHz; 155 scans. (b) The simulated spectrum for the cw-EPR species of (a) with $A_{||} = 504.0$ MHz and $g_{||} = 1.9460$ was generated using the program QPOWA with the experimental conditions above.

RESULTS

Effect of βK167 Mutations on Photoautotrophic Growth. The relative abilities of the wild-type and mutant strains of *Chlamydomonas reinhardtii* to grow under photoautotrophic conditions are shown in Table 1. All of the mutants affected the rate of photoautotrophic growth significantly. The initial doubling time for wild type was 10 h while that of each mutant was about 60 h, although photoautotrophic growth was sustained longer with βK167H than with the other mutants.

Effects of βK167 Mutations on CW-EPR and ESEEM Spectra of VO^{2+} Bound to Site 3 of CF_1-ATPase. Figure 1a shows parallel features of the continuous wave EPR (cw-

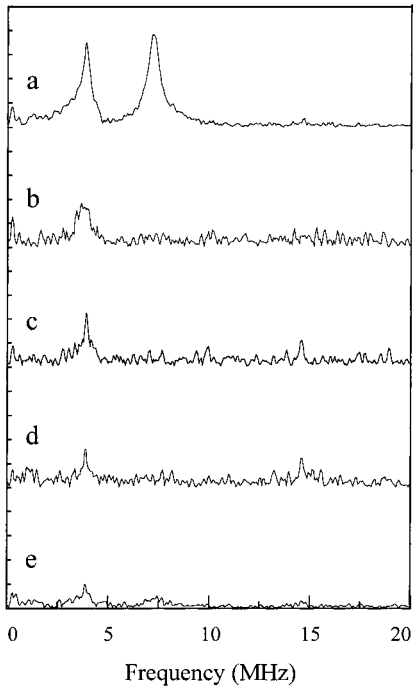

FIGURE 2: Three-pulse ESEEM of VO^{2+} bound in the absence of nucleotide to site 3 of latent CF_1-ATPase from (a) wild-type, (b) βK167G, (c) βK167H, (d) βK167L, and (e) βK167C mutants of *Chlamydomonas reinhardtii*. The conditions were: field setting, 3435 G; microwave frequency, 9.67 GHz; pulse repetition rate, 1000 Hz; interpulse time τ, 136 ns; data points, 512. These spectra are the Fourier transforms of the corresponding data in Figure 3.

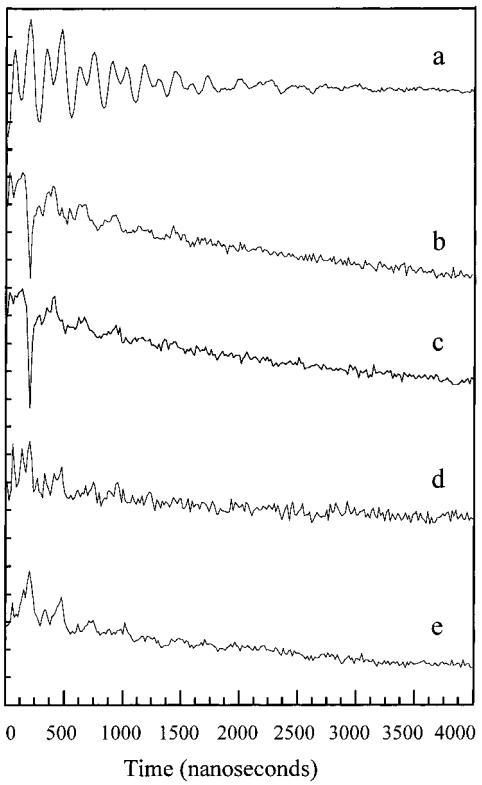

FIGURE 3: Spin echo envelope of VO^{2+} bound in the absence of nucleotide to site 3 of latent CF_1-ATPase from (a) wild-type, (b) βK167G, (c) βK167H, (d) βK167L, and (e) βK167C mutants of *Chlamydomonas reinhardtii*. The conditions were: field setting, 3435 G; microwave frequency, 9.67 GHz; pulse repetition rate, 1000 Hz; interpulse time τ, 136 ns; data points, 512.

EPR) spectrum of VO^{2+} bound in the absence of nucleotide to site 3 of CF_1-ATPase from wild-type *Chlamydomonas reinhardtii*. The types of groups coordinated at the equatorial positions of VO^{2+} strongly affect the magnitudes of $A_{||}$ and $g_{||}$. These quantities determine the average spacing between the parallel transitions, and the magnetic field position of the center of the parallel transitions, respectively. Of these parameters, the parallel hyperfine coupling, $A_{||}$, shows the largest and most easily discerned changes as a function of the types of groups that serve as equatorial ligands to the metal.

The simulated spectrum that provides the best fit is shown in Figure 1b using $A_{||} = 504.0$ MHz and $g_{||} = 1.9460$ as summarized in Table 2. These parameters are consistent with three equatorial oxygen ligands from carboxyl groups and one equatorial nitrogen ligand from an amine. This EPR species closely resembles that observed when VO^{2+} is bound to site 3 of spinach CF_1-ATPase (*31*).

The precision of the values of $A_{||}$ and $g_{||}$ depends on several factors that affect signal-to-noise, including the sensitivity of the EPR cavity, the concentration of the enzyme-bound VO^{2+}, and the number of scans that were signal-averaged. The probable error inherent in the determination of $A_{||}$ by simulation is approximately 0.1 MHz (*39*).

Figure 2a shows the frequency domain ESEEM spectrum of VO^{2+} bound to site 3 of CF_1-ATPase from wild-type *Chlamydomonas reinhardtii*. ESEEM can detect interactions between the electron spin of VO^{2+} ($S = 1/2$) and nuclear spins such as ^1H ($I = 1/2$) and ^{14}N ($I = 1$) if they are sufficiently close to the bound VO^{2+}. The ESEEM spectrum for wild-type CF_1-ATPase contained two intense nuclear transition frequencies at 3.9 and 7.1 MHz. These frequencies are indicative of an ^{14}N nucleus from an amine bound in an equatorial position to the VO^{2+} (*32*, *40*).

The effects of *C. reinhardtii* βK167 mutations on the VO^{2+} cw-EPR and ESEEM spectra were examined. This residue is analogous to the P-loop lysine that is the closest amino side chain to the metal in the catalytic sites of the MF_1-ATPase crystal structure (*4*). The ESEEM spectrum for βK167G CF_1-ATPase contained a nuclear transition at 3.9 MHz, similar to that of wild type (Figure 2b). However, the intensity of this feature was much less than that observed in the wild type. The 7.1 MHz peak was not reliably reproduced in ESEEM spectra of the mutant. The 3.9 MHz transition is assigned to ^{14}N. The other available nonzero spin nucleus, ^1H, would not give rise to a transition in this region unless there were a very strong ^1H-superhyperfine coupling. Such a coupling is normally undetectable by X-band ESEEM.

The frequency domain ESEEM spectra described above were computed using the Fourier transform of the spin echo envelope (Figure 3). Modulation depth of the spin echo envelope is proportional to the fraction of VO^{2+} ions contributing to the electron spin echo that are interacting with an $I > 0$ nucleus, such as an ^{14}N nucleus. As shown in Figure 3a, the wild-type enzyme with VO^{2+} bound to site 3 displays relatively deep modulations. A pattern can easily be discerned in this envelope suggesting that most or all VO^{2+} ions that contribute to the cw-EPR signal are coupled to an equatorial coordinating ^{14}N nucleus. However, modulation depths from VO^{2+} bound to the βK167G mutant CF_1-ATPase are much less intense (Figure 3b). This is a good indication that only a small percentage of the VO^{2+} bound to the enzyme gives

Table 2: ^{51}V-Hyperfine Tensors of CW-EPR Species of VO^{2+} Bound to Site 3 of CF_1 from Wild Type and βK167 Mutants of *Chlamydomonas*

	experimental parameters[a]		calculated parameters[b]					
genotype	$A_{\|\|}$ (MHz)	$g_{\|\|}$	$A_{\|\|}$ (MHz)	$g_{\|\|}$	most probable VO^{2+} equatorial ligands			
wild type	504.0	1.9460	504.25	1.9445	RNH_2	RCOO	RCOO	RCOO
K167C	498.5	1.9470	498.78	1.9455	H_2O	ROH	RCOO	RCOO
K167G	489.0	1.9510	490.01	1.9475	ROH	RCOO	RCOO	RCOO
K167H	491.5	1.9465	490.01	1.9475	ROH	RCOO	RCOO	RCOO
K167L	498.5	1.9470	498.78	1.9455	H_2O	ROH	RCOO	RCOO

[a] Derived using QPOWA. [b] Calculated from eq 1.

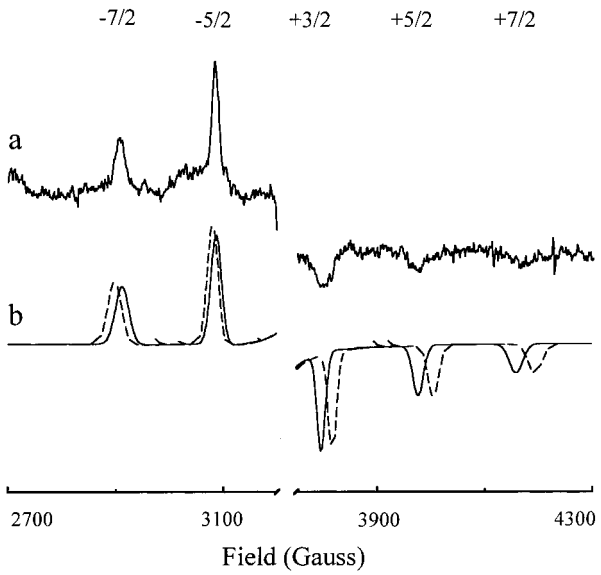

FIGURE 4: (a) Parallel regions of the cw-EPR spectrum of VO^{2+} bound in the absence of nucleotide to site 3 of latent CF_1-ATPase from the βK167G mutant of *C. reinhardtii*. One mole equivalent of VO^{2+} was added to 47 mg of βK167G-CF_1 as described under Experimental Procedures. EPR conditions were as follows: field modulation frequency, 100 kHz; modulation amplitude, 0.5 mT; sweep rate, 0.95 mT/s; time constant, 82 ms; microwave power, 2.0 mW; temperature, 125 K; microwave frequency, 9.660 GHz; 316 scans. (b) The simulated spectra of the mutant species with $A_{||}$ = 489.0 MHz and $g_{||}$ = 1.9510 (solid line) and wild type (dashed line) were generated as in Figure 1.

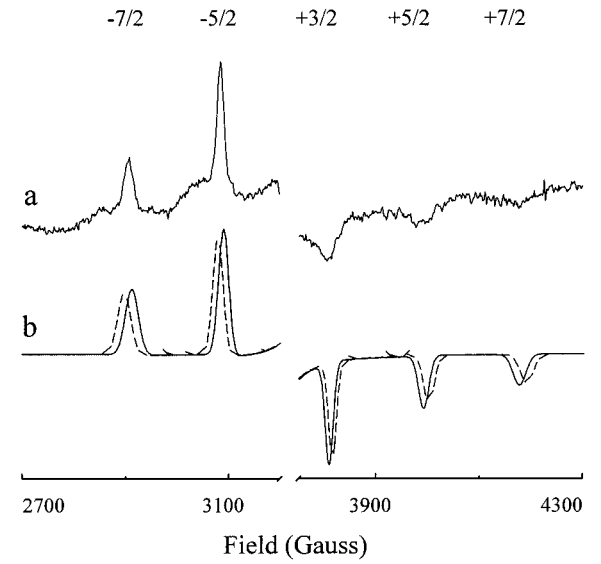

FIGURE 5: (a) Parallel regions of the cw-EPR spectrum of VO^{2+} bound in the absence of nucleotide to site 3 of latent CF_1-ATPase from the βK167H mutant of *C. reinhardtii*. One mole equivalent of VO^{2+} was added to 81 mg of βK167H CF_1 as described under Experimental Procedures. EPR conditions were as follows: field modulation frequency, 100 kHz; modulation amplitude, 0.5 mT; sweep rate, 0.95 mT/s; time constant, 82 ms; microwave power, 2.0 mW; temperature, 125 K; microwave frequency, 9.659 GHz; 301 scans. (b) The simulated spectra of the mutant species with $A_{||}$ = 491.5 MHz and $g_{||}$ = 1.9465 (solid line) and wild type (dashed line) were generated as in Figure 1.

rise to the 3.9 MHz transition shown in Figure 2b. The small percentage of VO^{2+} ions that are coupled to a ^{14}N nucleus most likely arise from adventitiously bound VO^{2+} to backbone or other nitrogens in the protein.

Upon the addition of VO^{2+} in the absence of nucleotide to site 3, the βK167G CF_1-ATPase showed a single cw-EPR species with ^{51}V-hyperfine coupling significantly smaller than wild type (Figure 4a). In Figure 4b, the simulated spectrum of βK167G (solid line) had values for $A_{||}$ and $g_{||}$ of 489.0 MHz and 1.9510, respectively. The simulation of the wild-type spectrum (dashed line) derived using the same microwave frequency as that used to obtain the experimental spectrum shows the differences between the wild-type and mutant spectra. The difference in $A_{||}$ between βK167G and wild type is 15.0 MHz. The exchange of an amine group for a hydroxyl group as an equatorial ligand would account for a change of 14.3 MHz. Therefore, the most probable ligand set that also gives the best fit to the data from βK167G contains a hydroxyl and three carboxyl oxygens as equatorial ligands (Table 2).

In the case of βK167H, the simulated spectrum had values of $A_{||}$ = 491.5 MHz and $g_{||}$ = 1.9465 (Figure 5b), resulting in a 13.5 MHz difference in $A_{||}$ between βK167H and wild type. The ligand set that gives the best fit to the data from βK167H contains a hydroxyl, a carboxyl oxygen, a water, and an imidazole group as equatorial ligands. However, the ESEEM spectrum for βK167H does not show nuclear transition frequencies consistent with an equatorially coordinating histidine (Figure 2c). Instead, the ESEEM spectrum is similar to that of βK167G. The shallow modulation depths that are observed with this mutant (Figure 3c) indicate that the majority of bound VO^{2+} is not coordinated to ^{14}N. Thus, the most probable ligand set for VO^{2+} bound to site 3 of βK167H is a hydroxyl and three carboxyl oxygens as equatorial ligands with a hydroxyl group substituting for the amine group (Table 2). The $A_{||}$ value of this ligand set is only 1.5 MHz from that observed for βK167H.

Figures 6a and 7a show the parallel transitions of the cw-EPR spectrum of VO^{2+} bound to site 3 of CF_1-ATPase containing the βK167L and βK167C mutations, respectively. In each case, a single cw-EPR species was observed for which the ^{51}V-hyperfine coupling was smaller than wild type. Figures 6b and 7b compare the simulated spectra of the wild type (dashed lines) to those of the mutants (solid lines). The $A_{||}$ values of both βK167L and βK167C were 5.5 MHz

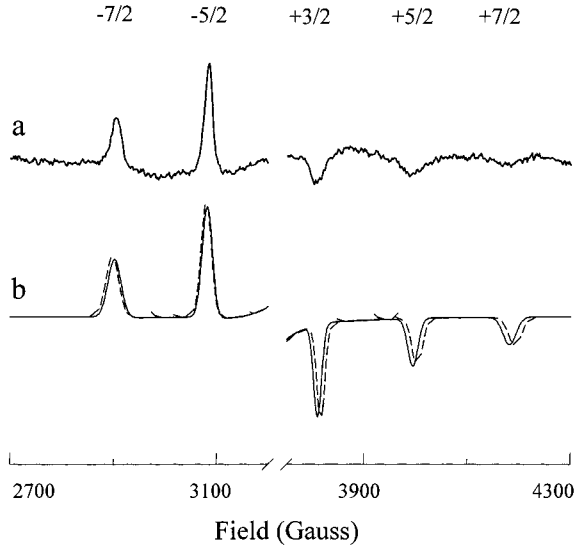

FIGURE 6: (a) Parallel regions of the VO^{2+} EPR spectrum of VO^{2+} bound in the absence of nucleotide to site 3 of latent CF_1-ATPase from the βK167L mutant of *C. reinhardtii*. One mole equivalent of VO^{2+} was added to 52 mg of βK167L-CF_1 as described under Experimental Procedures. EPR conditions were: field modulation frequency, 100 kHz; modulation amplitude, 0.5 mT; sweep rate, 0.95 mT/s; time constant, 82 ms; microwave power, 2.0 mW; temperature, 125 K; microwave frequency, 9.442 GHz; 256 scans. (b) The simulated spectra of the mutant species with $A_{||} = 498.5$ MHz and $g_{||} = 1.9470$ (solid line) and wild type (dashed line) were generated as in Figure 1.

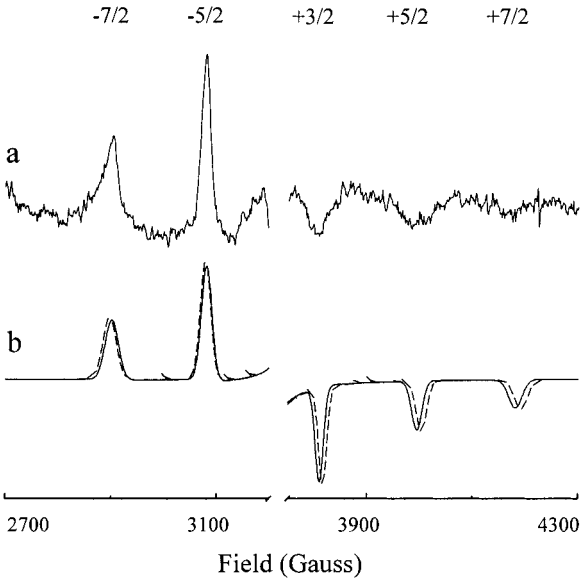

FIGURE 7: (a) Parallel regions of the cw-EPR spectrum of VO^{2+} bound in the absence of nucleotide to site 3 of latent CF_1-ATPase from the βK167C mutant of *C. reinhardtii*. One mole equivalent of VO^{2+} was added to 91 mg of βK167C-CF_1 as described under Experimental Procedures. EPR conditions were as follows: field modulation frequency, 100 kHz; modulation amplitude, 0.5 mT; sweep rate, 0.95 mT/s; time constant, 82 ms; microwave power, 2.0 mW; temperature, 125 K; microwave frequency, 9.656 GHz; 285 scans. (b) The simulated spectra of the mutant species with $A_{||} = 498.5$ MHz and $g_{||} = 1.9470$ (solid line) and wild type (dashed line) were generated as in Figure 1.

smaller than the wild type (Table 2). The most probable ligand set that gives the best fit to the data from βK167L and βK167C contains oxygens from a hydroxyl, a water, and two carboxyl groups as equatorial ligands.

The three-pulse ESEEM of VO^{2+} bound to site 3 of CF_1-ATPase from the mutations βK167L and βK167C are shown in Figures 2d and 2e. The effects of these mutations on the ESEEM spectra were similar to βK167G and βK167H in that there are significant decreases in ^{14}N transition amplitudes. As with the other mutants, the total modulation depths in the time domain were much shallower than those that originated from the wild-type enzyme (Figure 3d,e). These data concur with the evidence from the cw-EPR spectra that essentially none of the bound VO^{2+} in the βK167 mutants was coordinated by nitrogen at an equatorial position.

DISCUSSION

The data presented here indicate that the putative amine ligand in the free-metal-bound form at catalytic site 3 is the P-loop lysine of the β-subunit. In the CF_1-ATPase of *Chlamydomonas reinhardtii*, every βK167 mutant changed the cw-EPR and ESEEM spectra as compared to wild type.

Histidine has been reported to serve as an equatorial ligand to F_1-ATPase-bound VO^{2+} in addition to an amino group (*41*, *42*). In the data presented here, there is evidence of an equatorially coordinating lysine, but no evidence for an equatorial histidine. In this study, we have described the metal-binding environment of the lowest-affinity catalytic site with VO^{2+} bound under conditions in which the remaining catalytic sites contain Mg^{2+}-nucleotide at pH 8. The equatorially coordinating histidine has been observed at pH 7 when VO^{2+} is bound to a high-affinity catalytic site, such as when VO^{2+} was bound to empty thermophilic F_1-ATPase (*41*), and when VO^{2+} was bound to CF_1-ATPase from spinach that has been dialyzed to deplete bound metal-nucleotide (*42*). The crystal structure of bovine mitochondrial F_1-ATPase shows no histidine residues close to the catalytic metal-binding sites, suggesting that any histidine metal ligands would result from nonspecific binding of VO^{2+}. It is noteworthy, based on the results presented here, that ^{14}N modulations can be detected in an ESEEM spectrum from a small fraction of the total amount of bound VO^{2+} (Figures 2 and 3).

The cw-EPR data presented here from VO^{2+} bound without nucleotide to site 3 of mutant CF_1-ATPase provide insight into the metal ligand set responsible for the free-metal-bound form of the enzyme. Table 2 shows the values of $A_{||}$ and $g_{||}$ derived from QPOWA that best fit the cw-EPR spectrum and the values of $A_{||}$ and $g_{||}$ calculated from eq 1 that give the closest fit to the experimental data. When VO^{2+} without nucleotide was bound to site 3 of latent *C. reinhardtii* CF_1-ATPase from wild type, the value of $A_{||}$ was 504.0 MHz. The free-metal-bound species with a best fit equatorial ligand set that contains one lysine has been previously reported in spinach CF_1-ATPase (*31*). However, the value of $A_{||}$ was reported to the nearest 10^{-4} cm^{-1}, which is equivalent to about a 3 MHz range. Consequently, the $A_{||}$ value of 504.0 MHz here for *C. reinhardtii* CF_1-ATPase is at the lower limit of the range of MHz values corresponding to $A_{||} = 169 \times 10^{-4}$ cm^{-1} reported for spinach. Based on the data presented here, the other equatorial ligands to VO^{2+} in addition to the P-loop lysine are oxygens from three carboxyl groups.

The highly conserved P-loop motif contains the consensus sequence GXXXXGKT, in which the threonine is known to be a metal ligand while the lysine hydrogen-bonds to the

γ-phosphate oxygens of bound ATP. Site-directed mutations of the P-loop lysine of the β-subunit in CF_1-ATPase to a glycine, cysteine, histidine, or leucine side chain significantly affected the photoautotrophic growth of *Chlamydomonas reinhardtii*, which is consistent with previous characterizations of P-loop lysine mutations (*20*, *43*−*45*). Upon deactivation of CF_1-ATPase, Mg^{2+}-ADP is bound to a high-affinity catalytic site in an improper manner. This entrapped Mg^{2+}-ADP is postulated to be part of the regulatory mechanism to minimize ATP hydrolysis by CF_1F_0-ATP synthase. Stabilization of the entrapped Mg^{2+}-ADP by the binding of free Mg^{2+} at the low-affinity site 3 may represent another step in this regulatory mechanism (*23*). The results presented here indicate that when Mg^{2+} is bound at site 3, the P-loop lysine is an equatorial ligand, thereby suggesting a regulatory role for βK167.

Previously, mutations of amino acid residues were found to change the ^{51}V-hyperfine parameters of VO^{2+}-ATP bound to catalytic site 3 of *C. reinhardtii* CF_1-ATPase. In the latent form of the enzyme, the VO^{2+}-nucleotide complex bound to site 3 gives rise to EPR species B ($A_{||} = 497.5$ MHz, $g_{||} = 1.9475$) (*30*). In this conformation, the Walker homology B aspartate (βD262) is an equatorial metal ligand (*27*), but the P-loop threonine (βT168) is not (*28*). Conversely, the activated form of site 3 (EPR species C: $A_{||} = 456.5$ MHz, $g_{||} = 1.9575$) contains βT168 but not βD262 as an equatorial metal ligand (*27*, *28*). These results suggest that an important step in the conversion of species B to C that takes place upon activation of CF_1-ATPase is the replacement of βD262 as an equatorial ligand by βT168. Consequently, βD262, a residue known to be important for catalysis as a metal ligand in site 1 (*20*, *29*, *46*), also contributes to the nonfunctional, regulatory metal-binding conformation in site 3. In a similar manner, the contribution of the P-loop lysine at catalytic site 3 as a metal ligand in the absence of nucleotide allows this residue to serve a regulatory role via the stabilization of entrapped Mg^{2+}-ADP at the high-affinity catalytic sites.

REFERENCES

1. Weber, J., and Senior, A. E. (1997) *Biochim. Biophys. Acta 1319*, 19−58.
2. O'NeaI, C. C., and Boyer, P. D. (1984) *J. Biol. Chem. 259*, 5761−5767.
3. Frasch, W. D., and Selman, B. R. (1982) *Biochemistry 21*, 3636−3643.
4. Abrahams, J. P., Leslie, A. G. W., Lutter, R., and Walker, J. E. (1994) *Nature 370*, 621−628.
5. Bianchet, M. A., Hullihen, J., Pedersen, P. L., and Amzel, L. M. (1998) *Proc. Natl. Acad. Sci. U.S.A. 95*, 11065−11070.
6. Weber, J., Bowman, C., and Senior, A. E. (1996) *J. Biol. Chem. 271*, 18711−18718.
7. Frasch, W. D. (1994) in *The Molecular Biology of Cyanobacteria* (Bryant, D., Ed.) pp 361−380, Kluwer, Dordrecht, The Netherlands.
8. Smith, J. P., and Boyer, P. D. (1976) *Proc. NatI. Acad. Sci. U.S.A. 73*, 4314−4318.
9. Schumann, J., and Strotmann, H. (1980) in *Proceedings of the 5th International Photosynthesis Congress* (Akoyunoglou, G., Ed.) Vol. 2, pp 881−892, Balban, Philadelphia, PA.
10. Dunham, K. R., and Selman, B. R. (1981) *J. Biol. Chem. 256*, 212−218.
11. Zhou, J. M., Xue, Z., Du, Z., Melese, T., and Boyer, P. D. (1988) *Biochemistry 27*, 5129−5135.
12. Jault, J.-M., and Allison, W. S. (1993) *J. Biol. Chem. 268*, 1558−1566.
13. Jault, J.-M., and Allison, W. S. (1994) *J. Biol. Chem. 269*, 319−325.
14. Jault, J.-M., Matsui, T., Jault, F. M., Kaibara, C., Muneyuki, E., Yoshida, M., Kagawa, Y., and Allison, W. S. (1995) *Biochemistry 34*, 16412−16418.
15. Digel, J. G., Kishinevsky, A., Ong, A. M., and McCarty, R. E. (1996) *J. Biol. Chem.* 271, 19976−19982.
16. Jault, J.-M., Dou, C., Grodsky, N. B., Matsui, T., Yoshida, M., and Allison, W. S. (1996) *J. Biol. Chem. 271*, 28818−28824.
17. Hochman, Y., Lamir, A., and Carmeli, C. (1976) *FEBS Lett. 61*, 255−259.
18. Murataliev, M. B., Yakov, M. M., and Boyer, P. D. (1991) *Biochem. Biophys. Res. Commun. 63*, 894−899.
19. Hochman, Y., and Carmeli, C. (1981) *Biochemistry 20*, 6287−6292.
20. Senior, A. E., and Al-Shawi, M. K. (1992) *J. Biol. Chem. 267*, 21471−21478.
21. Bulygin, V., Syroshkin, A., and Vinogradov, A. (1993) *FEBS Lett. 328*, 193−196.
22. Shobert, B. (1998) *Eur. J. Biochem. 254*, 363−370.
23. Digel, J. G., Moore, N. D., and McCarty, R. E. (1998) *Biochemistry 37*, 17209−17215.
24. Boyer, P. D. (2000) *Biochim. Biophys. Acta 1458*, 252−262.
25. Bruist, M. F., and Hammes, G. G. (1981) *Biochemistry 20*, 6298−6305.
26. Shapiro, A. B., Huber, A. H., and McCarty, R. E. (1991) *J. Biol. Chem.* 266, 4194−4200.
27. Hu, C.-Y., Chen, W., and Frasch, W. D. (1999) *J. Biol. Chem. 274*, 30481−30486.
28. Chen, W., LoBrutto, R., and Frasch, W. D. (1999) *J. Biol. Chem. 274*, 7089−7094.
29. Chen, W., Hu, C.-Y., Crampton, D. J., and Frasch, W. D. (2000) *Biochemistry 39*, 9393−400.
30. Houseman, A. L. P., LoBrutto, R., and Frasch, W. D. (1994) *Biochemistry 33*, 10000−10006.
31. Houseman, A. L. P., Morgan, L., LoBrutto, R., and Frasch, W. D. (1994) *Biochemistry 33*, 4910−4917.
32. Zhang, C., Markham, G. D., and LoBrutto R. (1993) *Biochemistry 32*, 9866−9873.
33. Walker, J. E., Saraste, M., Runswick, M., and Gay, N. J. (1982) *EMBO J. 1*, 945−951.
34. Nadanaciva, S., Weber, J., and Senior, A. E. (1999) *J. Biol. Chem. 274*, 7052−7058.
35. Hu, C.-Y., Houseman, A. L. P., Morgan, L., Webber, A. N., and Frasch, W. D. (1996) *Biochemistry 35*, 12201−12211.
36. Houseman, A. L. P., LoBrutto, R., and Frasch, W. D. (1995) *Biochemistry 34*, 3277−3285.
37. Chasteen, N. D. (1981) in *Biological Magnetic Resonance* (Berliner, L., and Reuben, J., Eds.) pp 53−119, Plenum Press, New York.
38. Hamstra, B. J., Houseman, A. L., Colpas, G. J., Kampf, J. W., LoBrutto, R., Frasch, W. D., and Pecoraro, V. L. (1997) *Inorg. Chem. 36*, 4866−4874.
39. Chen, W., and Frasch, W. D. (2001) *Biochemistry* (in press).
40. LoBrutto, R., Hamstra, B. J., Colpas, G. J., Pecoraro, V. L., and Frasch, W. D. (1998) *J. Am. Chem. Soc. 120*, 4410−4416.
41. Zimmermann, J.-L., Amano, T., and Sigalat, C. (1999) *Biochemistry 38*, 15343−15351.
42. Zimmermann, J.-L., Schneider, B., Morlet, S., Amano, T., and Sigala, C. (2000) *Spectrochim. Acta, Part A: Mol. Biomol. Spectrosc. 56A*, 285−299.
43. Parsonage, D., Al-Shawi, M. K., and Senior, A. E. (1988) *J. Mol. Biol. 263*, 4740−4744.
44. Senior, A. E., Wilke-Mounts, S., and Al-Shawi, M. K. (1993) *J. Biol. Chem. 268*, 6989−6994.
45. Omote, H., Maeda, M., and Futai, M. (1992) *J. Biol. Chem. 267*, 20571−20576.

BI002895Y